JAST, Vol. 13, No. 1, pp.

JAST
Journal of Aerospace Science and Technology

Science Article

Numerical Investigation of Aerodynamic Effects of Geometry and Sensor Distance on a Spherical Projectile

Kosar Mokhtari[1], Alireza Naderi[2*]
1-2: Aerospace Faculty, Malek-Ashtar University of Technology
*Lavizan, Tehran
Email: *naderi@mut.ac.ir

The present study investigates the flow around two tandem spheres and their aerodynamic optimization. In a systematic view, the downstream sphere is regarded as the projectile and the upstream sphere is the sensor. The aim of this study is to find the most appropriate configuration with lowest drag force. Therefore, the results of the effects of the center-to-center (CC) distance of the spheres, and the reduction of the sensor's diameter were investigated in 15 different cases. The results show that as the distance between the spheres decreases, the drag force of the spheres decreases too; reduction in the sensor's diameter would increase the projectile's drag while decreasing the sensor's drag. The highest effects on drag reduction were induced by constant distance between spheres and a change in sensor's diameter. Consequently, in the last stage of the study, the adjoint solution of the FLUENT software was used to reduce the drag of the whole set through optimization of the sensor frontal hemisphere. However, due to systematic limitations, only the shape of the forepart of the sensor can be changed. Since the sphere is a bluff body, efficient options are needed for the adjoint optimization algorithm and it's worth noting that the optimized shape in each case is different from other cases. The highest drag reduction happened in the case with a CC distance of 2.5 m and sensor diameter of 0.75 m. Furthermore, the case with CC distance of 1m and sensor diameter of 0.25 is the only case after optimization in which simultaneously the drag force of both spheres has been reduced.

Keywords; *bluff body, adjoint optimization, tandem spheres, drag reduction*

Introduction

Since the flow around bluff bodies, is observable in most of the aerodynamic shapes and structures and projectiles both separately and especially collectively in various conditions and positions, its investigation is indispensable and of utmost importance [1]. Investigating the nature of the flow around tall structures in a range, e.g., bridge piers, oil platforms, etc. is just a simple case of multi-cylindrical arrangements existing in our environment. The simplest arrangement can be found in double (side by side) or tandem arrangements. Due to flow separation and existence of vortices, analyzing the nature of the

1 . Holder of Master of Science
2 Assistant professor,(Corresponding author)

Received Date: 12 Nov. 2020
Accepted Date: 12 Dec. 2020

bluff body would not be without complexity. The existence of multiple bluff bodies formed in close proximity to one another, interaction effects of vortices, boundary layer, adverse pressure gradients, and separation points can also contribute to the intricacy of the analysis [2]. In significantly low Reynolds numbers, no instances of flow separation are seen. With the increase of the Reynolds number, the flow is separated from the surface and a pair of symmetrical vortices are formed in the back of the body. As the Reynolds number increases, the dimensions of the these vortices increase as well; with the increase of Reynolds number the extended vortices oscillate, collapse and are shed in the wake region.

Literature review

Due to the importance and high-applicability of the bluff bodies, especially the sphere, numerous researchers studied the nature of the flow around the sphere. A brief list of previous experimental studies conducted on this subject includes: Allen (1900), Arnold (1911), Shakespear (1914), Wieselsberger (1922-1923), Liebster (1927), Lunnon (1928), Schmiedel (1928), Moller (1938), Davis (1945), Pettyjohn and Christiansen (1948), Gunn and Kinzer (1949), Maxworthy (1965), Goin and Lawrence (1968), Pruppacher and Steinberger (1968), Beard and Pruppacher (1969), Rimon and Cheng (1969), Bailey and Hiatt (1971-1972), Dennis and Walker (1971), Roos and Willmarth (1971), Achenbach (1972), Vlajinac and Covert (1972), and Hartman et al. (1994). Of these works, Wieselsberger (1922), Maxworthy (1965), Goin and Lawrence (1968), Pruppacher and Steinberger (1968), Beard and Pruppacher (1969), Rimon and Cheng (1969), Bailey and Hiatt (1971-1972), and Achenbach (1972) have presented their data only in graphical form, hence accessing their precise data is impossible. By omitting the imprecise and defective data of some of these researchers, the results of drag coefficient according to Reynolds number can be displayed as a classic graph as shown in Fig. 1 [3].

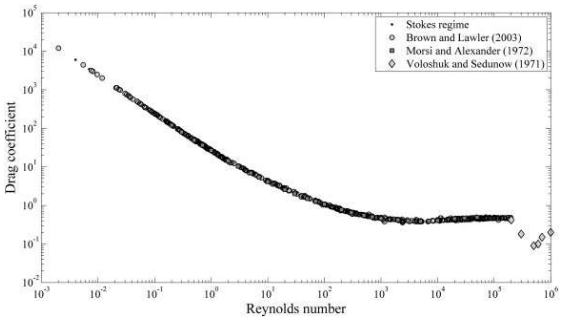

Fig. 1. Variations of the drag coefficient with Reynolds numbers based on experimental results

In the subsequent years, due to the prove relationship between the values of drag coefficient and the Reynolds number flow, researchers also began to present mathematical relations for predicting the drag coefficient. Over the last decade, some researchers have also attempted to estimate the drag of flow around spheres via CFD software.

Bluff bodies have higher drag values compared to streamlined or aerodynamic bodies. Consequently, drag reduction is highly important in these bodies, a goal that can be achieved through flow control and optimization. By changing the surface shape of the body, optimization methods tend to reduce drag value.

Over the past decades, many researchers have focused on the flow and drag value of a sphere; calculating the drag value by means of wind tunnels and numerical codes. Afterwards it was time for studies that investigated sphere shape change and drag reduction.

Choi et al. (2004) conducted a study on the active control of flow over a sphere at Re=10^5 for drag reduction using blowing and suction from a slot on the sphere surface. Their considered forcing frequency range was 1 to 30 times greater than the natural vortex-shedding frequency. The disturbances from the high-frequency forcing grow inside the boundary layer and delay the first separation while maintaining laminar separation, and they grow further along the separated shear layer and high momentum in the free stream is entrained toward the sphere surface, resulting in the reattachment of the flow the delay of the main separation. Then the reverse flow region is significantly reduced and finally as the Reynolds number increases, the drag forcing would decrease.

Choi et al. (2005) investigated the effects of dimples on the surface of a sphere in flow separation and drag reduction. They presented a mechanism that suggested dimples on a sphere such as golf-ball dimples trigger shear layer instability along the separating shear layer, resulting in generation of large turbulence intensity in the downstream. As a result, dimples delay the main separation. A similar mechanism (using high-frequency suction and blowing) was observed in the flow reduction over a smooth sphere. This flow-control strategy can be used for drag reduction on bluff bodies such as spheres and cylinders [6].

Continuing their researchers about nature of flow around bluff body, choi et al. (2010) investigated the effect of free-stream turbulence (FST) on the flow over a sphere. This experimental investigation of the effects FST on the flow was done at the Reynolds numbers of $0.5 \times 10^5 - 2.8 \times 10^5$. The results of this study showed that FST triggers the boundary layer instability above the sphere surface and delays the separation. Once the laminar separation bubble occurs, the disturbances both from the boundary-layer instability and FST trigger the shear layer instability. Then high momentum is entrained toward the sphere surface and the separated flow is reattached, forming a separation bubble on the sphere surface. Due to high momentum near the sphere surface, the main separation is delayed and the drag is reduced. The critical Reynolds number, at which the drag coefficient decreases rapidly, decreases as the FST intensity increases. With increasing Reynolds number, the first separation point moves downstream, but the reattachment and main separation points are nearly fixed, resulting in a constant drag coefficient. This indicates that forming a separation bubble on the sphere surface can reduce the drag coefficient. The reduced drag coefficient would remain constant as the separation bubble disappears. [7].

Niazmand and Anbarsooz (2010) conducted a study on the effects of convection on cooling down two circular cylinders in free-stream flows. The Reynolds number was set at 150 and the distance between the cylinders was varied between 1-5. The unsteady flow and the vortices formed in the back of the cylinders, as well as aerodynamic coefficients, all cause instability in heat transfer parameters including Nusselt number, which in turn reduces thermal efficiency. It was shown that since the upstream cylinder is in contact with free-stream and no vortices are formed in front of it, its heat transfer rate is equal to that of a single cylinder. However, the heat transfer rate of the downstream is 80% lower than the heat transfer value of a single cylinder. The Nusselt number for the downstream cylinder is 10 times lower than the upstream cylinder [8].

A numerical study of the dynamics and stability of the flow past two cylinders sliding along a wall in tandem configuration for Reynolds numbers between 20 to 200 was conducted by Rao et al. (2012). The experiments were conducted in small to large separation distances. As the distance between the cylinders reduces and they are almost tangent, the nature of the flow is similar to larger single bodies. Instability in drag coefficient is lower in downstream cylinder than the upstream one. It was also seen that by increasing cylinders distance (to the extent that streamlines becomes steady before reaching the downstream cylinder) in different Reynolds numbers, the drag coefficient value for intermediate regimes for the cylinders get closer and closer, approaching to a constant value. In three-dimensional modes, the increase of Reynolds number adds to the instability of the flow [9].

In an experimental study, Zhou et al. (2014) investigated flow past a circular cylinder with smooth, grooved and dimpled surface in 8 different Reynolds numbers ranging from 7.4×10^3 to 8×10^3. Drag and lift forces on the cylinders were measured using a piezoelectric load cell in conjunction with measurements of the wake flow pattern using digital Particle Image Velocimetry (PIV) for some cases. The results reveal that the grooved and dimpled cylinders produce a lower mean drag than that of a smooth cylinder. lower mean drags are observed in greater Reynolds numbers. The mean reduction of the grooved cylinder is ranged from 18% to 29%, while that of the dimpled cylinder is from 10% to 30%. The contour plots of Reynolds stress and turbulent kinetic energy also indicate that the strength of vertex shedding becomes weaker due to the presence of the grooved or dimpled surfaces [10].

Flow over a bluff body is a common and significant case for engineering sciences. Oruc (2016) conducted a research titled *Strategies for the applications of flow control downstream of a bluff body*. In addition to referring effective flow-

control methods, Oruc also highlighted the advantages and disadvantages of these techniques. In his investigations, Oruc classified the methods of flow-control into two groups, namely active control and passive control. His results indicated that passive control techniques of flows over a bluff body are significantly easier and more practical compared to active control method which may be more effective in flow control. Oruc also claims that the results of his study can also be used as an insightful and exhaustive reference for techniques of flow control over a bluff body. His paper also includes a review of major results of previous works in the field [11].

Pinelli et al. (2016) conducted a study aimed at controlling the wake behind a circular cylinder. first, a sparse layer of hairy filaments with same mounting angle was formed at the back of the cylinder. their results proved that increasing the angle between two symmetrically placed rows of filaments would improve the aerodynamic efficiency ratio. The experiment was repeated in the three-dimensional cylinder with more filaments. For experiments in Reynolds number range of $5000 \leq Re \leq 31000$, adding filament rows in the back of the cylinder, proved to reduce drag, turbulence and instability of control, and resonance of aeroelastic forces [12].

As it was already mentioned in the literature, drag force is significantly important in a bluff body such as sphere, and once another sphere is placed in a tandem configuration in front of the main sphere, the nature of the flow over the bluff body changes, consequently affecting the drag force of the set. This study investigates the behavior of the flow around two tandem spheres. The distance and the diameter of the upstream sphere are changed to relatively investigate the effects of the existence of the other sphere on the downstream sphere (projectile). Finally, through using the adjoin algorithm, the shape of the upstream sphere is optimized and as a result the drag force is reduced. Due to systematic limitations, the drag was reduced only by changing the frontal hemisphere in the adjoint algorithm. With the present investigation conducted in this study and systematic considerations, changing the shape of the frontal cylinder would be focused on. With the optimization and change of the frontal half of the upstream sphere, flow separation is delayed, hence the pressure in the back of the sphere is reduced which would in turn result in reduction of drag force.

In all cases of the experiments, first the flow equation was solved and after achieving convergence, the adjoint optimization algorithm was solved. The results of this study would be applicable as an investigation of optimization of the shape and structure of a projectile (downstream sphere) along with a sensor (upstream sphere).

Governing Equations

the governing equations of the flow in the two-dimensional Cartesian system and Eulerian frame include averaged-continuity and momentum equations. The governing equations are not closed-form since they include Reynolds stress expressions. One way to close the system of the governing equations is to rewrite Reynolds stresses like molecular viscosity stresses of fluids. In the rewritten stresses, a new stress coefficient is created and they can be modeled. Each of these models propose different equations for the calculation of the turbulent stress tensor. The two-equation SST k-ω turbulence model is one of these models that will be used in this numerical solution. All of the closed equations of continuity and momentum, as well as the turbulence model are mentioned in the reference [13].

The adjoint equations also present the I cost function which is known as a measure for aerodynamic performances like drag coefficient or the lift to drag ratio. In this function the flow about the airfoil would depend on the flow field variable of w, and the geometrical variable, X. (1) says;

$$I = I(w, X) \qquad (1)$$

Since w depends on X, a slight change in the geometrical aspects can change the cost function, resulting in

$$\delta \mathrm{I} = \left[\frac{\partial \mathrm{I}}{\partial w}\right]^T \delta w + \left[\frac{\partial \mathrm{I}}{\partial X}\right]^T \delta X \qquad (2)$$

The first term is ratio of the changes of δw in flow field and the second term shows the direct effects of the surface changes. If the governing equations over flow are written as (3), then the changes in R can be written as equation (4).

Journal of Aerospace Science and Technology
Vol. 13/ No. 1/ Winter- Spring 2020

$$R(w,X) = 0 \quad (3)$$

$$\delta R = \left[\frac{\partial R}{\partial w}\right]\delta w + \left[\frac{\partial R}{\partial X}\right]\delta X \quad (4)$$

By introducing a Lagrange multiplier ψ, the δI can be rewritten as (5).

$$\delta I = \left[\frac{\partial I}{\partial w}\right]^T \delta w + \left[\frac{\partial I}{\partial X}\right]^T \delta X - \psi^T\left(\left[\frac{\partial R}{\partial w}\right]\delta w + \left[\frac{\partial R}{\partial X}\right]\delta X\right) \quad (5)$$

Or we can have equation (6)

$$\delta I = \left\{\left[\frac{\partial I}{\partial w}\right]^T - \psi^T\left[\frac{\partial R}{\partial w}\right]\delta w\right\} + \left\{\left[\frac{\partial I}{\partial X}\right]^T - \psi^T\left[\frac{\partial R}{\partial X}\right]\delta X\right\} \quad (6)$$

Ψ is chosen to satisfy the adjoint equation, so that (7) could be written as

$$\left[\frac{\partial R}{\partial w}\right]\psi = \left[\frac{\partial I}{\partial w}\right] \quad (7)$$

Then the changes in I can be defined as

$$\delta I = G\ \delta X \quad (8)$$

Where,

$$G = \left[\frac{\partial I}{\partial X}\right]^T - \psi^T\left[\frac{\partial R}{\partial X}\right] \quad (9)$$

Then with respect to the equations, δI is independent of δw. As a result, in each cycle of the processes, redesigning the governing equations is only solved once through the adjoint equation and the G changes vector is independent of the number of design variables. In conclusion after calculating the vector of changes, the vector can be used to help the geometrical shape optimization [13].

The objective function is valuable numerical function that measures the efficiency and performance. In the present article the considered objective function is the drag coefficient minimization.

$$J = D \quad (10)$$

Primary Considerations for Numerical Solution

Figure 1 is a three-dimensional snapshot of the centroid section of the domain. It also shows the boundary conditions of the flow as well the how the spheres are positioned.

For preliminary numerical solution, domain size, grid sensitivity, time steps and numerical validation are needed. By selecting different domains of different size, the drag of the sphere was measured. Finally, a domain was selected where the center of the sphere was in a 20 meters distance from the front and surrounding boundaries as well as a 30 meters distances from the downstream boundary, all due to insignificant effect on the drag value. For the purpose of assessing the sensitivity to the grid size, a number of different grids with boundary layers sorted from large to short were selected and the drag force of all these cases were measured. finally, a grid consisting of 800K cells with a y+≤1 was chosen.

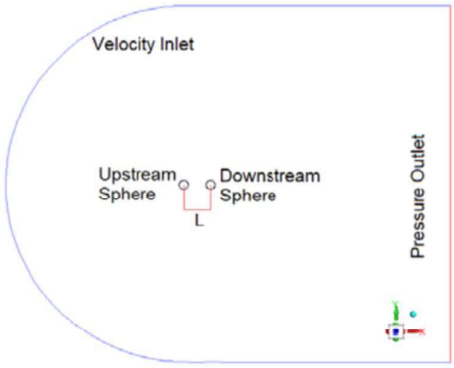

Figure 1 – centroid section of the solution domain and the possible boundary conditions

Although the flow around the sphere is unsteady in *Re* =1000, the temporal changes disappeared in the wake. The drag of the unsteady solution was investigated through various time steps and the results were compared to the steady solution results. Figure 2 presents the results of the unsteady solution. The drag coefficient of the single sphere in steady flow is 0.5370. As it can be seen, there is a small 0.0003 difference in the drag coefficient of steady vs. unsteady flow in time step of 0.025. On the other hand, since in shape optimization the focus is on the forepart of the sphere which is less affected by the wake, the steady solution would be used for comparison and optimization investigations.

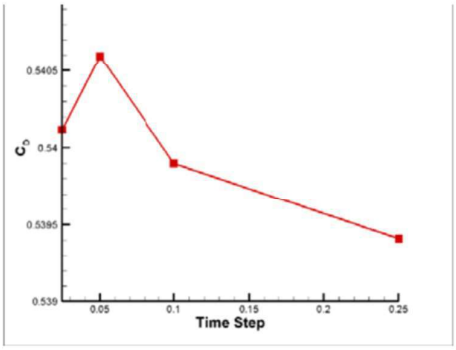

Figure 2 – Results of the unsteady solution in different time steps

As it was mentioned earlier, a reliable graph of drag coefficients around a sphere has been produced. For the purpose of validation, this drag coefficient graph is used in this numerical solution, as presented in figure 3. Since the results of the present study in *Re* = 1000 are very close and similar to the results of the previous studies, the results of this numerical investigation are validated.

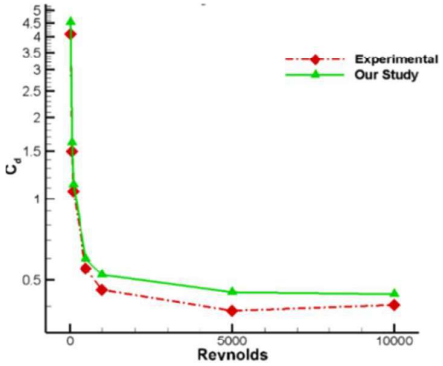

Figure 3 – Comparing of this numerical results with the results of previous experimental studies

Results

The aim of the current study is to investigates the aerodynamic effects of an upstream sphere (sensor) on the drag force of downstream sphere (projectile), as well as finding the minimum drag force for the whole set. For this reason, the diameter of sensor (upstream sphere) and the center-to-center, CC distance of the two spheres were changed. Overall, 15 different cases were investigated. The measured Reynolds number for the downstream sphere (projectile) which had a diameter of 1 meter, was *Re*=1000.

In all these cases where the downstream sphere's (projectile) diameter remained a constant of amount 1 meter and the two sphere's CC distance as well as the diameter of upstream sphere (sensor) kept changing, the drag coefficient was measured. Figure 4 presents the changes in drag force of both spheres in cases where the sensor's diameter stayed 0.5 m but the two sphere's distance kept changing. As it can be seen, by increasing the distance between the spheres, the drag force relatively increases. The drag force of the upstream sphere (projectile) does too but the drag of the downstream sphere (sensor) reaches an asymptotic state and becomes constant.

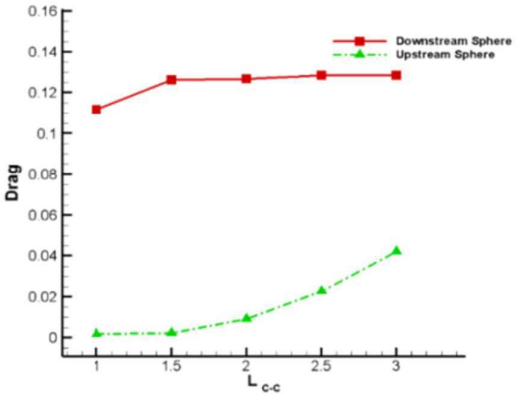

Figure 4 – The effect of CC distance change in the sphere drag, sensor sphere's diameter = 0.5 m

Likewise, the drag was measured in cases where the spheres remained in a constant distance, yet diameter factor of the upstream sphere (sensor) kept changing. Figure 5 shows the changes in drag in cases where the CC distance of the two spheres is 3 m, but the diameter of the sensor changes. As it can be seen in the figure, by increasing the sensor sphere's diameter, the drag force increases in the upstream sphere (sensor) whereas it decreases in the downstream sphere (projectile).

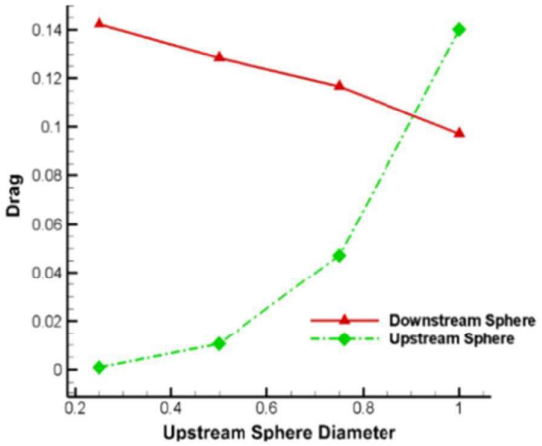

Figure 5- Spheres drag where sensor's diameter changes, and CC distance is 3m.

Figure 6 presents the amount of drag force in different cases of diameter and CC distances change on a chart. In this figure, the amount of drag force for the sensor and projectile has been presented both separately and tandemly. The displayed configurations have been designed in a way that the sum of drag force is from to minimum to maximum. The minimum drag force for the sphere was recorded in a case that the spheres' CC distance as well the diameter of the projectile were both 1m but the senor's diameter to be 0.25m. the maximum amount of drag was also seen in cases where the spheres' CC distance was 6m but the diameter of both sensor and projectile was 1m.

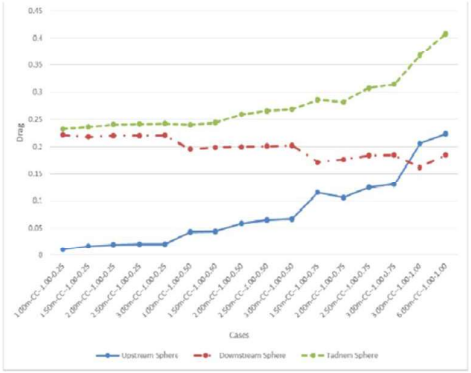

Figure 6 – Comparison of simultaneous effects of CC distance and diameter on drag forces.

To easily detect different cases, their names are chosen in a manner that showed both the distance and diameter of the two spheres and are shown in the following table:
The first number form the left shows the distance of the spheres

- The letter *m* has been used to indicate meters
- The letters *cc* show center-to-center distance
- The second number is the projectile's diameter
- And the last number is the sensor's diameter.

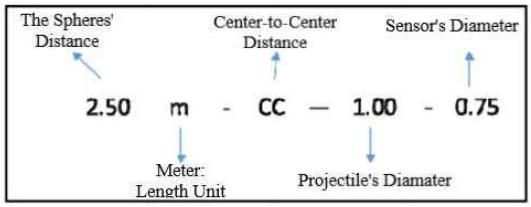

In the present study, three objectives for drag reduction can be defined; reducing the sensor's drag or the projectile's or the sum of the drag of both spheres. In this stage first in the case where the CC was 3m and sensor's diameter was 1m, the three objectives were investigated and the amount of drag reduction was compared. With the produced results, a path of decreasing the sensor drag was proceeded.
Table 1 shows the results of the investigation of changes in drag force in the specified objectives. The green numbers which are desirable show drag reduction and numbers in red show increasing drag forces. The results show that when the objective is reducing the projectile drag, shape optimization takes place in a way that it would finally lead to an increase in the force for the whole set. However, this is in contrast with the ultimate goal of selecting these objectives, which is drag reduction in the whole set. As it was mentioned, the objective of reducing the sensor drag shows the best results.

Table 1 – results of optimization in three different objectives

Summative drag	Projectile drag	Sensor drag	Objective
-3.96	5.13	-11.11	Sensor drag
11.27	-6.50	25.31	Projectile drag
-2.24	4.95	-7.90	Summative drag of both spheres drag

14 cases were optimized using the adjoin solution, the results of them can be found in Figure 7 & 8. In most cases, after optimization the drag force of the projectile (Figure 8) has increased in contrast to the sensor drag (Figure 7). However, in most cases after optimization took place, the drag force of the whole set was reduced.

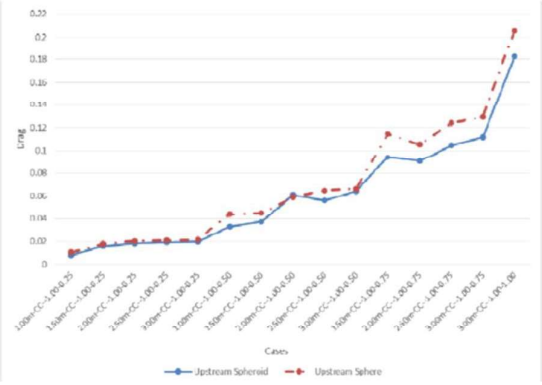

Figure 7 –comparison of the sensor drag in cases with sphere and spheroidal shapes

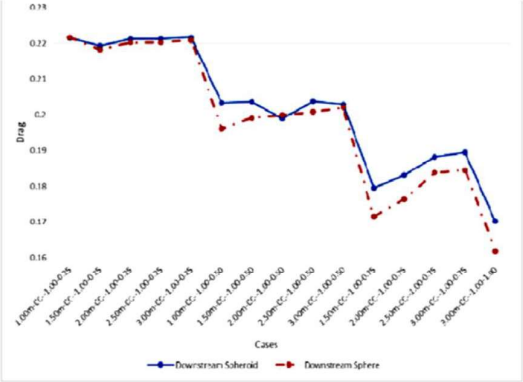

Figure 8 – Comparison of projectile drag in cases with sphere and spheroidal shapes

By comparing the results from decreasing the distance with diameter decreasing, the lowest amount of drag after changing the diameter and the distance was observed in the case where the spheres CC distance was 1m and the sensor diameter was 0.25 m; likewise, the highest observed drag was seen in the case where the spheres where CC distance was 6m and the sphere diameter was 1m. The results of optimization highlight that the highest drag reduction was observed in cases where CC distance was 1m and a sensor diameter of 0.25 & 0.5 m. In addition, the highest amount of drag reduction for the whole set was observed where CC distance was 2.5 m and the sensor diameter was 0.75 m.

Figure 9 presents the changes in the shape of the sphere in the process of shape optimization for a single case. To present more comprehensible results, the geometric grid of the surface in four different stages of optimization are presented in this figure. The pressure contours of the system with the lowest amount of drag force can be seen in Figure 10. The highest points of pressure are on the projectile nose. In Figures 9 & 10, the sensor's diameter is 0.25m and the CC distance is equal to 1m.

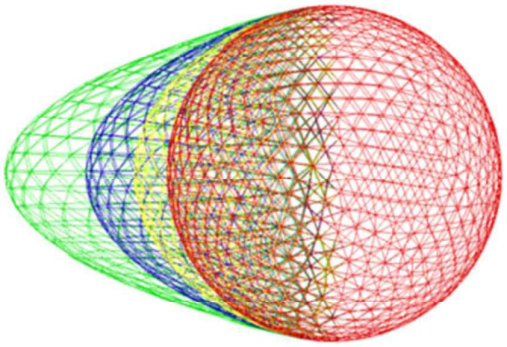

Figure 9 – Shape changes of sensor in different optimization stages.

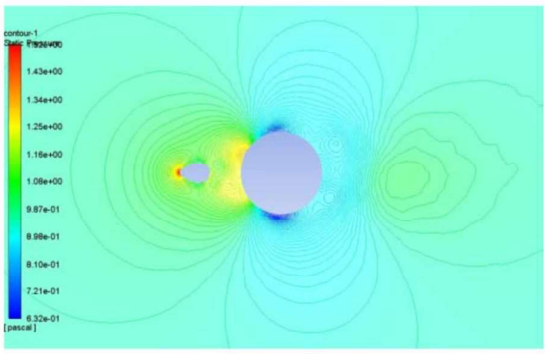

Figure 10 – Pressure contour of the field after optimizing the shape of the sensor.

Conclusion

This study investigated the amount of drag force in two tandem spheres, the projectile and the sensor. Accordingly, the distance between the spheres and the size of the sensor were subject to change. Furthermore, for the purpose of drag reduction, the shape of sensor's side that was against by the flow was optimized. The results of the study highlight that;

- Steady solution can be applied for comparisons needed for drag reduction
- A decrease in the CC distance would result in drag reduction of both spheres and consequently drag reduction for the whole set.

- Channing the sensor's diameter causes drag reduction for the sensor but it would increase the drag force for the projectile.
- Decreasing the sensor's diameter has a more primary effect on the drag reduction of the set.
- The lowest amount of drag force was observed in the case where both the CC distance and diameter of the sensor were changed and CC distance was 1m and the sensor's diameter was 0.25m.
- The adjoint method conducts the sensitivity analysis and defines the necessary shape change to reach the objective function. As it was evident, in different cases the amount of drag force (as the objective function of the optimization) is also different; hence the influence of adjoint method and the amount of shape change are different for each case.
- The highest amount of observed drag reduction after optimization was seen in a case where CC distance was equal to 2.5 meters and the sensor's diameter was 0.75 m.
- The only case after optimization in which the drag force of both the sensor and projectile was reduced, was the case where the CC distance spheres were 1 meter and sensor's diameter was 0.25.

References

P. W. Bearman, "Bluff body flows applicable to vehicle aerodynamics," Journal of Fluids Engineering, Vol. 102, no. 3, pp. 265-274, 1980.

D.I., Greenwell, 2011. Modelling of static aerodynamics of helicopter underslung loads. *The Aeronautical Journal, 115*(1166), pp.201-219.

P. P. Brown and D. F. Lawler, "Sphere drag and settling velocity revisited," Journal of Environmental Engineering, Vol. 129, no. 3, pp. 222-231, 2003.

R. B. Neyshabouri, S. A. A. Salehi, and G. Ahmadi, "Development of empirical models with high accuracy for estimation of drag coefficient of flow around a smooth sphere: An evolutionary approach," Powder Technology, Vol. 257, pp. 11-19, 2014.

S. Jeong, "Active control of flow over a sphere for drag reduction at a subcritical Reynolds number," Journal of Fluid Mechanics, Vol. 517, pp. 113-129, 2004.

J. Choi, W. Jeon, and H. Choi, "Mechanism of drag reduction by dimples on a sphere," Physics of Fluids, Vol. 18, no. 4, p.041702, 2006.

Kwangmin Son, "Effect of free-stream turbulence on the flow over a sphere," Physics of fluids, Vol. 22, no. 4, p.045101, 2010.

H. Niazmand, M. Anbarsooz, Slip flow over micron sized particles at intermediate Reynolds number, Mechanical Engineering, Vol. 40, No. 2, pp. 67-76, 2010.

Rao, A., Thompson, M.C., Leweke, T. and Hourigan, K. "Dynamics and stability of the wake behind tandem cylinders sliding along a wall. Journal of Fluid Mechanics, Vol. 722, pp. 291-316, 2013.

Zhou, B., Wang, X., Guo, W., Gho, W.M. and Tan, S.K.,"Experimental study on flow past a circular cylinder with rough surface," Ocean Engineering, Vol. 109, pp. 7-13, 2015.

V. Oruc, "Strategies for the applications of flow control downstream of a bluff body," Flow Measurement and Instrumentation, Vol. 53, pp. 204-214, 2017.

Pinelli, A., Omidyeganeh, M., Brücker, C., Revell, A., Sarkar, A. and Alinovi, E., "The PELskin project: part IV-control of bluff body wakes using hairy filaments," Meccanica, Vol. 52, no. 7, pp. 1503-1514, 2017

A. Jameson and S. Kim, "Reduction of the adjoint gradient formula for aerodynamic shape optimization problems," AIAA journal, Vol. 41, no. 11, pp. 2114- 2129, 2003